TEMPERATURE MEASUREMENTS OF AN IMPLOSION FOCUS*

T. Saito, A. K. Kudian** and I. I. Glass

Institute for Aerospace Studies, University of Toronto

Toronto, Canada

Spectroscopic temperature measurements were made at the focal point of imploding shock waves in the UTIAS implosion chamber, which has a 20-cm diameter hemispherical cavity. The chamber was filled with a stoichiometric H_2-O_2 gas mixture at different initial pressures (14 ∿ 68 atm). The mixture was ignited at the origin by an exploding wire generating an outgoing detonation wave which reflected at the chamber wall as an imploding shock wave (gas-runs). Additional experiments where an explosive shell of PETN was placed at the hemispherical wall were also conducted. The shell was detonated by the impact of the reflected gaseous detonation wave at its surface, thereby generating an intense implosion wave (explosive-run). The temperatures were measured at the implosion focus using a medium quartz Hilger spectrograph with an eight photocell polychromator attachment over the visible wavelength range. The measured radiation intensity distributions were fitted to blackbody curves. The temperatures were 10,000 ∿ 13,000 K for gas runs, and 15,000 ∿ 17,000 K for explosive runs. The continuous spectra from photographic film and the measured emissivities, which were very close to unity, confirmed that the plasma was a blackbody. Numerical studies using the random choice method (RCM) and classical strong-shock theory were used to analyse the flows in the entire range of the implosion process. Real-gas effects and radiation losses were also considered. The results were compared with the experimental data and good agreement was obtained.

1. INTRODUCTION

The UTIAS explosive-driven implosion chamber has been used in several research areas since it was conceived by Glass (Ref. 1) in the early 1960's. The extremely high pressures and temperatures generated at the focus of implosions were utilized for driving projectiles to hypervelocities (Ref. 2), as a shock-tube driver (Ref. 3), and to produce diamonds (Ref. 4). Currently, experimental studies were done on deuterium-deuterium fusion reactions and

*This work was supported by the Canadian Natural Sciences and Engineering Research Council, the U.S. Air Force under Grant AFOSR-77-3303, and the U.S. Army Rosearch Office.

**Senior Physicist, Fraser Papers Inc., Thorold Division, Thorold, Ontario.

measurements of the resulting neutrons and gamma rays (Ref. 5).

The conditions produced by imploding spherical shock waves were first obtained by Guderly (Ref. 6). His self-similar solutions, however, deal only with very strong shock waves. They do not allow for any characteristic lengths, such as the chamber radius in the present problem. Consequently, in the present study, the conditions in the chamber were calculated by combining the numerical results of the RCM and solutions using strong-shock theory.

The principle of operation of the UTIAS 20-cm dia implosion chamber can be understood by referring to Fig. 1. The hemispherical chamber is filled with a $2H_2+O_2$ mixture at high pressure (14 ~ 68 atm for pure gas runs and 27 atm for explosive runs). The gas is ignited by exploding a fine nickel wire (0.13 mm dia x 1 mm long) at the origin of the hemisphere creating an outgoing detonation wave which is reflected at the hemispherical-chamber wall and then converges on the origin as an imploding shock wave. For an explosive run, a PETN explosive shell bonded against the wall of a copper-carrier liner is ignited upon reflection of the detonation wave and further reinforces the imploding shock wave. The imploding wave is again reflected at the origin leaving behind an extreme high-pressure-temperature region. The objective of the present work was to measure the peak temperature of this region and compare the data with analysis.

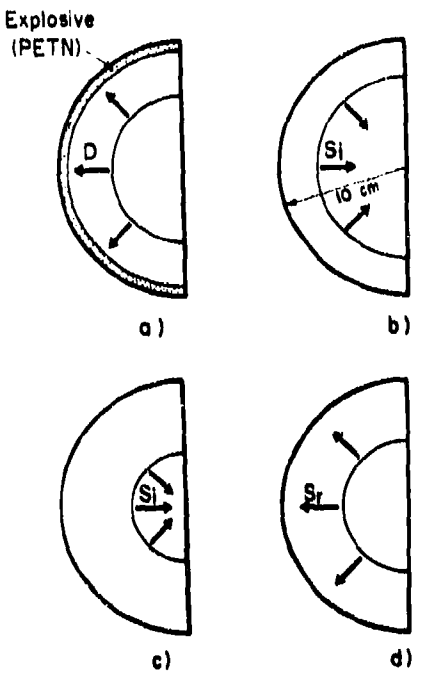

Fig. 1 Schematic of implosion chamber wave dynamics.

(a) Outgoing detonation wave in $2H_2+O_2$ mixture.
(b) Detonation wave reflects as a shock wave (or initiates the hemispherical PETN liner when used).
(c) Implosion phase onto the origin when the converging shock becomes very strong.
(d) Implosion reflects as an exploding shock wave leaving behind a high-pressure-temperature region.

In previous experiments, time-integrated (Ref. 7) as well as time-resolved colour-temperatures of the implosion focus made with large observing areas (3 x 9 mm) were found to be surprisingly low (4000 to 5000 K) (Ref. 8). In the present work, a much smaller observing area (0.55 mm dia) was used and time-resolved simultaneous measurements were made at eight wavelengths covering the visible region. Our temperature measurements are more precise (Ref. 11) and are in better agreement with expected values. Also, the emissivity of the radiating plasma was evaluated for the first time.

2. EXPERIMENTAL ARRANGEMENTS

The UTIAS implosion chamber consists of two massive front and rear plates held together by 32 large bolts (Ref. 9). A 20-cm dia hemispherical cavity is machined in the rear plate supporting a hemispherical copper liner. An explosive PETN package is manufactured on the inner surface of the copper liner for explosive runs. The barrel, which holds the Plexiglas observing window, the gas inlet and the exploding wire are installed in the front plate. For explosive runs, a 30-degree conical liner plate is added to the front plate to guard the chamber from any serious mechanical damage due to off-focus implosions (Ref. 10).

A 0.13-mm dia x 1-mm long nickel wire is exploded at the geometrical centre of the chamber by discharging a 1-μF capacitor charged to 21 KV. All spectroscopic observations were made with a Hilger medium-quartz spectrograph. For photographic work Kodak Plus-X pan film was used. For time-resolved photoelectric recording a photomultiplier attachment enabled simultaneous measurements at eight wavelengths (3900, 4148, 4391, 4710, 5123, 5629, 6328 and 7525 Å). The time-response of the system was about 0.1 μsec. The calibration of the photomultipliers was done in the conventional manner using a calibrated tungsten ribbon strip lamp.

For gas runs, a $2H_2+O_2$ gas-mixture was filled at different pressures (13.6, 27.2, 40.9, 54.5 and 68.1 atm). Thickness of 1.6 mm and 3.2 mm PETN explosive shells were used with a $2H_2+O_2$ gas-mixture of 27.2 atm initial filling pressure for explosive runs. These explosive shells weighed approximately 40g and 80g, respectively.

3. EXPERIMENTAL RESULTS

Pictures of the radiation spectrum of the first implosion pulse were taken to investigate the characteristics of the radiation with a rotating-disk shutter. Details of the operation of the shutter can be found in Refs. 7 and 11. It was found that the spectrum was completely continuous suggesting that the temperature of the radiating gas at the implosion focus can be determined by finding a blackbody curve of a certain temperature which fits best to the experimental data. The temperature measurements were carried out photoelectrically with the experimental set-up shown in Fig. 2. A brass mask with a small hole (0.55 mm dia) at the centre was placed on the window surface. The observing area was determined by the hole size and the width of the entrance slit of the spectrograph.

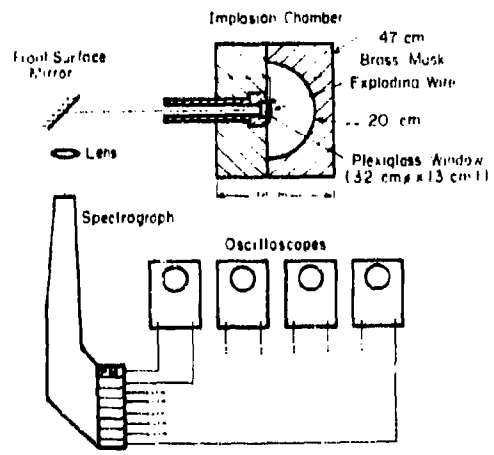

Fig. 2 Schematic diagram of experimental facility to study spherical implosions.

A typical oscillogram of a time-resolved measurement for a gas run is shown in Fig. 3. The recordings are strongly disturbed by the electromagnetic pick-up from the discharge system of the exploding wire. The interference disappears in about 30 μsec and the radiation intensity stays at a quite constant value until the first implosion wave comes back to the origin. The implosion time (the time between the ignition and the arrival of the implosion shock wave at the centre) was approximately 75 μsec for gas runs and 59 μsec and 56 μsec for explosive runs of 1.6 and 3.2 mm PETN layers, respectively. In gas runs some subsequent implosion pulses were observed although the radiation intensities were much lower than the first implosion pulse. The window broke about 500 ∿ 700 μsec after ignition for gas runs and about 18 μsec after the first implosion pulse for explosive runs.

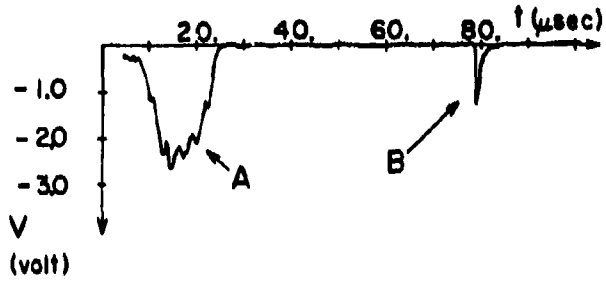

Fig. 3. Typical output signal from photomultiplier for a gas run. p_0 = 27.2 atm, λ = 5123Å.

A: Noise from discharging system + radiation from exploding wire.

B: Implosion pulse.

The radiation intensities at eight different wavelengths which cover the whole visible radiation range were measured for each run to eliminate the run-to-run fluctuation due to the variation in the degree of focussing.

The radiation intensity of a graybody at a given temperature T and wavelength λ_i is expressed as

$$I_{\lambda_i} = E \cdot B_{\lambda_i}(T) \tag{1}$$

where $B_{\lambda_i}(T)$ is the Planck law,

$$B_{\lambda_i}(T) = \frac{C_1}{\lambda_i^5} \frac{1}{\exp(C_2/\lambda_i T) - 1} \quad \frac{\text{erg}}{\text{cm}^3 \cdot \text{sec} \cdot \text{ster}} \tag{2}$$

with $C_1 = 1.191 \times 10^{-5}$ erg·cm^2·sec^{-1} and $C_2 = 1.4388$ cm K; E is the emissivity of the radiating gas. Under the condition $\exp(C_2/\lambda T) \gg 1$, $B_{\lambda_i}(T)$ can be replaced by the Wien approximation,

$$B_{\lambda_i}(T) \approx \frac{C_1}{\lambda_i^5} \exp\left(\frac{-C_2}{\lambda_i T}\right) \tag{3}$$

Substituting Eq. (3) into Eq. (1) results in

$$\ln\left(\frac{C_1}{I_{\lambda_i}\lambda_i^5}\right) = \frac{C_2}{T}\frac{1}{\lambda_i} - \ln E \tag{4}$$

Obtaining the intensities I_{λ_i} (i = 1, 2, ..., 8) experimentally, the temperature can be determined from the slope of the line which goes through the data points of a plot of the values of the left-hand side of Eq. (4) against the wave number $(1/\lambda_i)$. The emissivity can also be evaluated from the values at the intersection of the line with the vertical axis. However, after evaluating

some experimental data, it was found that the temperature range obtained at the implosion focus was above 10,000 K and the accuracy of Wien's approximation was poor. Therefore, in practice, the temperature and emissivity were varied to minimize the sum of the squares of deviations in the experimentally obtained intensities from the intensities given by Eq. (2). Typical results of a gas run and an explosive run are shown in Fig. 4. The results are presented taking advantage of Eq. (4), namely, the solid lines are drawn in such a way that their slopes and their intersections with the ordinate represent the temperature and emissivity obtained by using Planck's law and the data points are correspondingly corrected by a factor

$$F_{\lambda_1}(T) = 1 - \exp\left(\frac{C_2}{\lambda_1 T}\right) \tag{5}$$

which is simply the ratio of Planck's law to Wien's approximation.

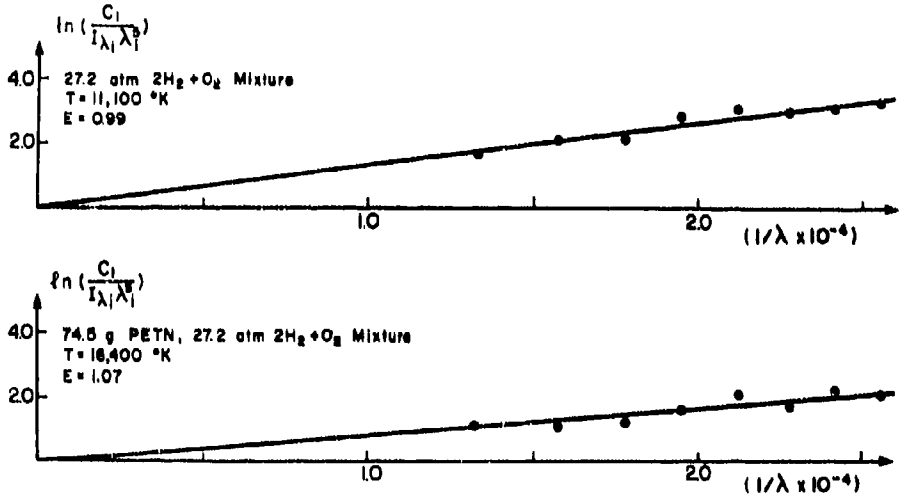

Fig. 4. Experimental results for a gas run and an explosive run.

It was found that the emissivity of the radiating gas was very close to unity except for the low initial pressure gas runs (p_0 = 13.6 and 27.2 atm) where the emissivities have a range of 0.7 ∿ 0.9.

4. ANALYTICAL PREDICTIONS

In the present study, the RCM was employed to calculate the imploding stage. Details of the RCM are available in Refs. 12 to 15. In the RCM, the waves are propagated statistically and the discontinuities such as shocks and contact surfaces appear as perfectly sharp fronts without any smearing, unlike finite-difference schemes using artificial viscosity. Self-similar solutions for constant speed spherically expanding Chapman-Jouguet (C-J) detonation waves in the detonation stage were calculated to give the initial conditions for the imploding stage (Ref. 16). The details of the numerical results from the RCM and strong-shock theory for gas runs and explosive runs are given in full in Ref. 11.

5. COMPARISON OF EXPERIMENTAL RESULTS AND THEORY

Figure 5 compares the experimental results and the expected average tem-

peratures over a 0.55-mm dia circular area at the origin. The calculated temperature depends on the position of the imploding shock wave. When the wave radius is larger than the radius of the observing area only the wave front can be seen through the window. When the imploding shock wave comes inside the observing area, not only the wave front but also the region behind the imploding shock wave is seen and the averaged temperature becomes lower than the temperature at the wave front. This arises from the rapidly falling temperature behind the implosion wave. As a result, the averaged temperature has a maximum when the radius of the imploding shock wave is slightly smaller than the radius of the observing area. The imploding shock radius at which this occurs is called R*, as shown on Fig. 5. In other words, there is a certain maximum observable temperature for a certain size of observing area no matter how small the imploding shock wave converges. This maximum temperature and the temperatures which are expected to be observed when the imploding waves are at different radii from the centre are also shown in Fig. 5. In principle, if it were possible to place the observing area exactly at the focus of the implosion then higher temperatures would be measured with decreasing mask hole size. However, in practice the size of 0.55 mm dia was found to be an optimum limit considering the time resolution of the present measuring system.

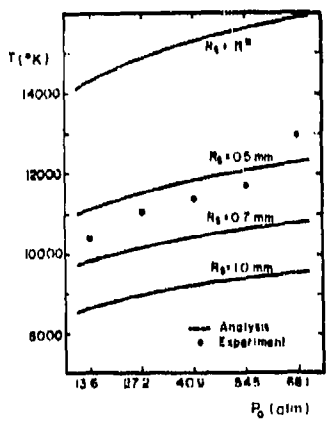

Fig. 5(a). Comparison of experimental results with analysis for gas runs.

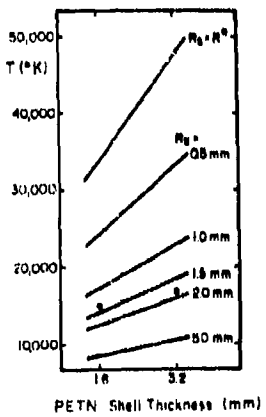

Fig. 5(b). Comparison of experimental results with analysis for explosive runs.

For gas runs the dependence of measured temperatures on the initial filling pressures agreed quite well with the analytical predictions although the absolute values of the temperatures were somewhat (∿ 20%) lower than the expected maximum temperatures. The lower values of the measured temperature can be attributed to the fact that the temperature behind the imploding shock front decreases rapidly. When the temperature is measured in a radial direction from a certain point ahead of the wave front, it would be lower than the front temperature. It would probably be a kind of averaged temperature of the region between the shock front and a certain point behind the front by about the same distance as the radiation mean free path. It has been calculated that, when the imploding wave radius R_g has converged to R* (∿ 0.25 mm, in Fig. 5), the temperatures at points 5 and 63μ behind the shock front are, respectively, 90 and 60% of the shock-front temperature.

For the explosive runs, the measured temperatures were much lower than the expected temperatures. Also the increase in the measured temperatures for increased PETN thickness was small compared with the analytical prediction.

Considering the much higher temperatures in explosive runs at the shock front than in gas runs, the so-called "screening effect" of the preheated gas layer ahead of the shock front (Ref. 17) is probably the reason for this phenomenon.

Although the measured maximum temperatures were relatively low and corresponding to large analytical radii for the imploding waves in explosive runs, the pressures obtained in explosive runs are much higher than in gas runs even for the highest initial gas pressure (p_o = 68.1 atm) as the window breaks much faster in explosive than in any gas runs. The final size of the implosion focus which gives the measured temperature obtained analytically is about 1.5 mm radius. The final pressure that would be obtained in an explosive run for this focal size corresponds to the pressure which would be obtained in a gas run of $p_o \sim 54$ atm when it converged to about 0.6 mm radius. However, the window breaks nearly 20-fold faster in the explosive runs, producing a pressure far beyond what can be produced in a gas run of 54 atm initial pressure. Despite the fact that the observed temperature remains at a low value, owing to the preheating of the gas ahead of the shock wave and becomes opaque with a surface temperature of about 17,000 K, the actual implosion focus continues to decrease to much smaller values (from the 1.5 mm radius). However, this has no effect on the measured temperatures as the preheated gas is opaque.

Although an appropriate perfect-gas analysis ($\gamma \sim 1.14$) was used throughout the present work, the approach appears quite reasonable. Flagg (Ref. 10) has shown that the isentropic exponent of the gas scarcely changes during the implosion and reflection stages ($\gamma \sim 1.14$) after investigating the numerical results of Brode (Ref. 18) who used an equation of state for a real gas for a burnt $2H_2+O_2$ mixture. The equilibrium compositions of the $2H_2+O_2$ system were calculated separately in the present study using the method of minimizing Gibbs' free energy (Ref. 19). It was noted that the effects of increasing temperature and pressure on dissociation and ionization compensate each other and no significant change in the composition occurred.

The radiation loss has also been estimated and it was found that the order of the loss compared to the energy flux into the shock-wave region due to the converging geometry, i.e., the inhomogeneous term of the energy equation in the lossless basic equations was negligibly small ($10^{-2} \sim 10^{-6}$), owing to the very high pressure and particle velocity ($p \sim 1.4 - 5.8 \times 10^4$ atm and $u \sim 12$-24 km/sec at R_s = 0.1 mm). Therefore, the radiation loss is not important for the present work.

In the most recent experiments (Ref. 5), where deuterium was used instead of hydrogen, production of neutrons and γ-rays from D-D reactions were observed. If this is the case then the final focus of the implosions could be very small, say the order of 10μ.

6. CONCLUSIONS

The continuous radiation spectra and the measured emissivities showed that the hot gases at an implosion focus from gas and explosive drivers radiate as blackbodies. The temperatures at the focal point of an imploding shock wave were measured spectroscopically in the visible region. For gas runs, the effect of the initial filling pressures on the temperature was small and 10,000 $\sim$ 13,000 K were measured when the initial pressure was increased from 13.6 to 68.1 atm. This dependence of the temperature agreed very well with analytical results. For explosive runs, the observed temperatures were 15,000 K for a 1.6-mm and 17,000 K for a 3.2-mm shell of PETN explosive. The measured temperatures in explosive runs were limited to 15,000 $\sim$ 17,000 K owing to the screening effect of the preheated layer ahead of the shock front, even though the imploding shock wave continued to converge. A high degree of

convergence was obtained despite the possible existence of bifurcation of the imploding shock waves due to the boundary layer developed on the flat surface and some of the unavoidable geometrical roughness of the chamber around the origin (which is not small, if we talk about a final focus in the micron range). It is even more remarkable if neutrons and γ-rays can be obtained (Ref. 5). Many additional investigations are still needed to settle the question of the actual final focal size and the physical conditions which exist there. Further details can be found in Ref. 11.

REFERENCES

1. I. I. Glass, "Appraisal of UTIAS Implosion-Driven Hypervelocity Launchers and Shock Tubes", in Prog. in Aerospace Sci., edited by D. Kuchemann, Vol. 13, pp. 223-291, Pergamon Press, Oxford and New York, 1972.
2. R. F. Flagg and I. I. Glass, "Explosive-Driven Spherical Implosion Waves", Phys. Fluids, 11, 10, pp. 2282-2284, 1968.
3. I. I. Glass, H. L. Brode and S. K. Chan, "Strong Planar Shock Waves Generated by Explosively-Driven Spherical Implosions", AIAA J. 12, 3, pp. 367-374, 1974.
4. I. I. Glass and S. P. Sharma, "Production of Diamonds from Graphite Using Explosive-Driven Implosions", AIAA J. 14, 3, pp. 402-404, 1976.
5. I. I. Glass and D. Sagie, "Application of Explosive-Driven Implosions to Fusion" (to be published).
6. G. Guderley, "Strong Spherical and Cylindrical Shock Waves in the Neighbourhood of the Center of the Sphere or the Axis of the Cylinder", Luftfahtforschung, 19, 9, pp. 392-412, 1942.
7. D. E. Roberts and I. I. Glass, "Spectroscopic Investigation of Combustion-Driven Spherical Implosion Waves", Phys. Fluids, 14, 8, pp. 1662-1670, 1971.
8. R. A. Roig and I. I. Glass, "Spectroscopic Study of Combustion-Driven Implosions", Phys. Fluids, 20, 10, pp. 1651-1656, 1977.
9. W. Czerwinski, "Structural Design and Development of UTIAS Implosion-Driven Launchers", UTIAS Report No. 153, 1971.
10. R. F. Flagg, "The Application of Implosion Wave Dynamics to a Hypervelocity Launcher", UTIAS Report No. 125, 1967.
11. T. Saito, "An Analytical and Experimental Study of the Temperatures at Implosion Foci Produced by Combustion and PETN-Explosives", University of Toronto Ph.D. Thesis, in progress.
12. J. Glimm, "Solution in the Large for Nonlinear Hyperbolic Systems of Equations", Comm. Pure Appl. Math. 18, pp. 697-715, 1965.
13. A. J. Chorin, "Random Choice Solution of Hyperbolic Systems", J. Comp. Phys. 22, pp. 517-533, 1976.
14. G. A. Sod, "A Numerical Study of a Converging Cylindrical Shock", J. Fluid Mech. 83, 4, pp. 785-794, 1977.
15. T. Saito and I. I. Glass, "Applications of Random-Choice Method to Problems in Shock and Detonation-Wave Dynamics", UTIAS Report No. 240, 1979.
16. J. H. Lee, R. Knystautas and G. G. Bach, "Theory of Explosions", McGill University, MERL Report 69-10, 1969.
17. Ya. B. Zel'dovich and Yu. P. Raizer, "Physics of Shock Waves and High-Temperature Hydrodynamic Phenomena", Vols. I and II, Academic Press, 1967.
18. H. L. Brode, "Theoretical Description of the Performance of the UTIAS Hypervelocity Launcher", Astronautica Acta. 15, pp. 301-309, 1970.
19. C. W. Stroud and K. L. Brinkley, "Chemical Equilibrium of Ablation Materials Including Condensed Species", NASA TN D-5391, 1969.